

Photofragmentation study of Cl₂ using ion imaging

Peter C. Samartzis, Ioannis Sakellariou,^{a)} Theodosia Gougousi, and Theofanis N. Kitsopoulos

Department of Chemistry, University of Crete and Institute of Electronic Structure and Laser, Foundation for Research and Technology-Hellas, 711 10 Heraklion-Crete, Greece

(Received 1 October 1996; accepted 25 March 1997)

The Cl(²P_{3/2}) and Cl(²P_{1/2}) photofragments produced by the photolysis of Cl₂ at ~3.5 eV, are detected using (3+1) and (2+1) resonance enhanced multiphoton ionization and their velocity distributions are measured using ion imaging. The measured photofragment translational energy distributions yield a bond dissociation energy of $D_0 = 2.474 \pm 0.020$ eV for ground electronic state Cl₂(X¹Σ_g). The angular distributions yield anisotropy parameters of $\beta(^2P_{3/2}) = -0.87 \pm 0.05$ and $\beta(^2P_{1/2}) = 1.78 \pm 0.05$ irrespective of the detection process. The branching ratio $[Cl(^2P_{1/2})]/[Cl(^2P_{3/2})]$ is estimated at $8 \pm 1\%$. © 1997 American Institute of Physics. [S0021-9606(97)00425-X]

I. INTRODUCTION

The ultraviolet absorption spectrum of molecular chlorine between 250 and 450 nm is continuous with its maximum occurring at ~330 nm. The spectrum has been attributed to transitions between the Cl₂(X¹Σ_g) ground electronic state and the purely repulsive ¹Π_u and B³Π_u excited electronic states. A correlation diagram between the atomic states of free Cl and the molecular electronic states of Cl₂ has been reported by Mulliken,¹ Herzberg,² Li *et al.*³ and Matsumi *et al.*,⁴ according to which the strong spin-orbit interaction in atomic chlorine mandates a Hund's case (c) description of Cl₂.⁵ Consequently, the proper notations for the molecular electronic states are 0_g⁺(X¹Σ_g), 1_u(¹Π_u), for the states correlating to Cl(²P_{3/2}) + Cl(²P_{3/2}), and 0_u⁺(B³Π_u) for the state correlating to Cl(²P_{3/2}) + Cl(²P_{1/2}).² In the remaining manuscript we will use Cl and Cl* to denote Cl(²P_{3/2}) and Cl(²P_{1/2}) respectively, following the same notation used by Matsumi *et al.*⁴

The 0_u⁺ ← 0_g⁺(X¹Σ_g) constitutes a parallel transition ($\Delta\Omega=0$) which implies that the maximum transition probability occurs when the molecular axis and the direction of the electric field are aligned. On the contrary, the 1_u ← 0_g⁺(X¹Σ_g) is described as a perpendicular transition ($\Delta\Omega=1$) in which case the maximum transition probability occurs when the molecular axis is perpendicular to the direction of the electric field. The nature of the transition probability coupled with the lifetime and the rotational period of the excited state, have a direct consequence to the angular distribution $I(\theta)$ of the photofragments, which is described by^{6,7}

$$I(\theta) = \frac{1}{4\pi} (1 + \beta P_2(\cos\theta)), \quad (1)$$

where β is called the anisotropy parameter ($-1 \leq \beta \leq 2$) and $P_2(\cos\theta)$ is the second Legendre polynomial. For a prompt dissociation $\beta = -1$ if the transition is perpendicular and $\beta = 2$ if a parallel transition is involved. Clearly, the shape of photofragment angular distribution can provide useful infor-

mation concerning the nature of the Cl₂ photodissociation process in this near ultraviolet region (275 to 450 nm).

Almost concurrently Busch *et al.*⁸ and Diesen *et al.*⁹ reported their results concerning the photodissociation of Cl₂ at 347.1 nm, both using photofragmentation translational spectroscopy. Although the angular distribution of the photofragments was not presented by Busch *et al.*, the authors reported that the maximum photofragment intensity occurred at right angles to the laser polarization direction, thus leading them to attribute the observed peak in the translational energy distribution solely to production of two Cl atoms. Diesen *et al.* presented the relative photofragment intensity at 9 angles and qualitatively compared their results to a $\sin^2(\theta)$ distribution. Although no translational energy distribution was reported they assigned their observations to formation of both Cl and Cl*, failing however to report the branching ratio between the two.

Using a multiphoton ionization (MPI) scheme to identify the nature of the photofragments¹⁰ Colson and co-workers³ studied the photodissociation of Cl₂ at 323.6 and 331.0 nm. In this one-color five-photon experiment, one photon was used to dissociate the Cl₂ molecule while the chlorine photofragments were ionized using (3+1) MPI. As no transition corresponding to Cl* was identified, the authors concluded that Cl atoms are produced exclusively during the Cl₂ photodissociation process.

Arikawa and co-workers¹¹ studied the photofragmentation of Cl₂ at 308 and 351 nm using Doppler spectroscopy. In this study, following the photolysis of the Cl₂ at each of the wavelengths mentioned above, both the Cl and Cl* were detected using (2+1) MPI.¹⁰ The authors concluded that the $[Cl^*]/[Cl]$ branching ratio is less than 0.01, while analyzing the Doppler line shapes for the Cl-atom MPI, they concluded that $-0.8 \leq \beta(^2P_{3/2}) \leq -1$. In a similar experiment, Kawasaki and co-workers⁴ reported anisotropy parameters and branching ratios for the entire 300 to 485 nm region. Below 370 nm the authors observe a strong propensity for Cl production as $[Cl^*]/[Cl] \approx 0.01$, while they report that this branching ratio becomes significant for $\lambda > 400$ nm reaching a maximum value of 0.47 at about 475 nm. More recently,

^{a)}Also at: Department of Physics, University of Crete.

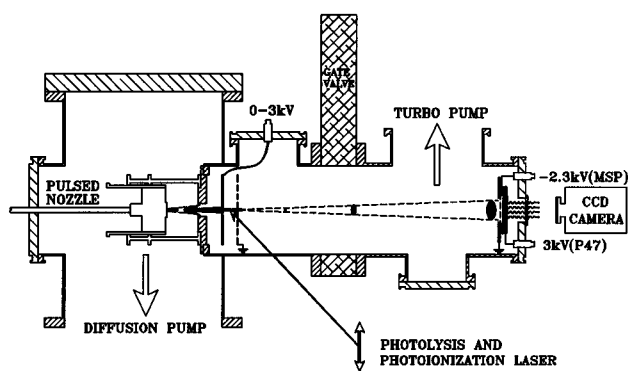


FIG. 1. A schematic of the experimental apparatus.

Hess and co-workers¹² have also studied the fine structure quantum yields from the dissociation of Cl₂ at ~ 235 nm, using a similar MPI detection scheme as in the above Doppler experiments and find that $[Cl^*]/[Cl] \approx 0.23$.

In this report we present our results concerning the velocity distributions (speed and angle) of the Cl and Cl* photofragments following the photolysis of Cl₂ at ~ 3.5 eV. The ion imaging technique we employed,^{13–15} combines: (a) MPI detection of the nascent products for spectroscopic identification. (b) Direct measurement of the photofragment angular distribution thus determining the anisotropy parameter. (c) Measurement of the Cl-photofragment translational energy distribution for directly determining product state distributions and branching ratios.

II. EXPERIMENT

A schematic of the photofragment imaging spectrometer used in this study is presented in Figure 1. The apparatus consists of two differentially pumped chambers: (i) the source region which is pumped by a baffled 3000 ℓ/s oil diffusion pump (Leybold, DI 3000) and (ii) the detector region which is pumped by a 600 ℓ/s turbo-molecular pump (Leybold, Turbovac 600). A gas sample containing 5% Cl₂ (Merck 99%) in He (Messer Greisheim 99.999%), is expanded into the source vacuum chamber via a home-built piezoelectrically actuated pulsed molecular beam¹⁶ operating at 20 Hz. A stagnation pressure of $P_0 \leq 1$ atm and a nozzle diameter of 0.8 mm are used in order to minimize cluster formation during the expansion. Approximately 5 cm from the nozzle orifice the expansion is skimmed using a $\varnothing 1.5$ mm skimmer (Beam Dynamics) which also serves as means of differentially pumping the two regions of the apparatus. Subsequently, the molecular beam is collimated using $\varnothing 0.8$ mm slit located 8 cm from the nozzle orifice. A uniform electric field is produced by two parallel stainless steel plates (outer-diameter 10 cm), one of which supports the collimating slit at its center (repeller electrode), while the other supports a very fine grid (333 lines/in., 70% transmittance, by Buckbee-Mears) over a center bore of $\varnothing 6$ cm (extractor electrode).

Midway between the repeller and extractor electrodes a laser beam generated by an excimer-pumped (Lambda Physik EMG 202, operating with XeCl) pulsed-dye laser (Lambda Physik FL2002, operating with DMQ), is focused onto the collimated beam of neutrals using a lens with a 20 cm focal length. In the one-color experiment, the photolysis laser pulse is also used for the (3+1) MPI of the nascent Cl and Cl* photofragments. The laser power is maintained at about 3–5 mJ/pulse in order to minimize space-charge effects from excessive ion production in the interaction region. In the two-color experiment the probe laser beam used for the (2+1) resonance enhanced multiphoton ionization (REMPI) of the Cl and Cl* photofragments is produced by frequency doubling the output of an excimer-pumped (Lumonics HyperX400, operating with XeCl) pulsed-dye laser (ELTO LT1233, operating with Coumarin 480), using a BBO crystal. The velocity distribution of the Cl-atom photofragments produces a Doppler energy shift in the resonant transition used for their (2+1) or (3+1) REMPI which is larger than the probe-laser bandwidth. Hence it is necessary to tune the laser in order to ensure that all photofragments are ionized with equal probability. Ions produced are accelerated along the axis of the machine towards a position-sensitive detector located approximately 45 cm from the interaction region. Ions of different masses are separated by time-of-flight during their field-free trajectory on route to the detector.

The home-built imaging detector consists of a single micro-sphere plate (MSP-50 by El Mul) coupled to a P47-phosphor-coated anode (Proxitronix) and has an effective diameter of 40 mm. Although the spatial resolution of the MSP plate (500–700 μm) is significantly less than that of the microchannel plate (~ 30 μm), the ultimate spatial resolution of this detector is determined by the extent of the interaction volume as determined by the width of the molecular beam. As the width of our molecular beam is 800 μm , the resolution of the MSP is not expected to degrade the ion image. Discrimination between the ions of interest and the undesired background ions is achieved by gating the detector through the application of a high-voltage pulse to the anode (amplitude = +3 kV, duration ≈ 150 ns). Atomic chlorine occurs in two isotopes with masses 35 and 37, respectively, which are readily resolved by their time-of-flight. The results presented in this report are obtained by gating our detector such that only $^{35}\text{Cl}^+$ ions are detected. The timing of the experiment is controlled using a pulse generator (DG535 by Stanford Research Systems) and is optimized by monitoring the ion signal which appears on a 100 MHz oscilloscope (Hameg HM1007) by capacitively coupling the MSP output-side voltage. During the “gated” operation, signal monitoring is stopped as the high voltage pulse applied to the anode will capacitively couple to the monitoring oscilloscope.

Images appearing on the phosphor anode are recorded using a charge-coupled-device (CCD) video camera (model 4910, by COHU Inc.), equipped with a 50 mm f1.4 lens and on-chip integration capabilities. Digitization of the camera output is controlled by a video frame grabber (DT55LC, by Data Translation). The limited dynamic range of the 8 bit

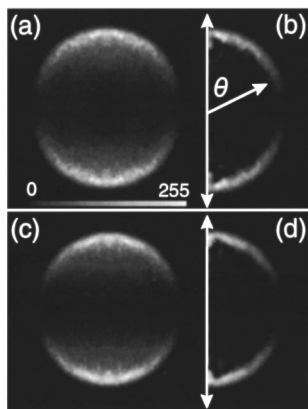


FIG. 2. (a) Data image of the Cl(²P_{1/2}) photofragment generated from the photodissociation of Cl₂ at 3.400 eV and detected using (2+1) REMPI. (b) Reconstruction of the data image in (a). (c) Data image of the Cl(²P_{1/2}) photofragment generated from the photodissociation of Cl₂ at 3.440 eV and detected using (3+1) REMPI. (d) Reconstruction of the data image in (c). Only half the image is presented in (b,d) since we have assumed azimuthal symmetry. The polarization direction of the photolysis laser is indicated by the arrow.

frame grabber is circumvented by performing essentially digital frame averaging. In other words, by maintaining low laser flux such that the number of ions generated per laser shot are 1–50, for typical frame integration times of the 5 s and 20 Hz laser operation, approximately 100 to 5000 particle positions are recorded over an area of $\sim 3 \times 10^5$ pixels. As long as each particle hit can be identified,¹⁷ the “dynamic range” of the frame grabber is irrelevant since the counts per position for each frame will be added together to form the complete image (analogous to photon counting). Background images are obtained either by tuning the photoionizing laser off-resonance or changing the timing of the laser pulse so that it arrives at the interaction region long after the molecular beam pulse has crossed this region. In this particular experiment the former of the two methods is used for obtaining background images.

III. RESULTS

In the one color experiment the photolysis energies 3.477 and 3.440 eV are chosen as they coincide with the three-photon resonant transitions $4s'(^2D_{5/2,3/2}) \leftarrow 3p^5(^2P_{3/2})$ and $4s'(^2D_{5/2,3/2}) \leftarrow 3p^5(^2P_{1/2})$ in the chlorine photofragments.¹⁸ In the two color experiment the photodissociation laser is 3.40 eV and the Cl and Cl* photofragments were ionized using two-photon resonant transitions $4p(^4D_{5/2}) \leftarrow 3p^5(^2P_{1/2})$ at 240.19 nm and the $4p(^4P_{3/2}) \leftarrow 3p^5(^2P_{3/2})$ 240.53.^{10,18,19} Since the mass of the photoelectron is negligible compared to the mass of the Cl atom, the three-dimensional (3D) velocity distribution of the post-ionized Cl⁺ ions will be identical to the 3D velocity distribution of the nascent Cl photofragments. By extracting all the Cl⁺ ions along a direction normal to the detector’s surface, we are in essence projecting the 3D velocity distribution onto a two-dimensional (2D) plane. The data images of the 2D projection of the 3D velocity distributions for the photofragments

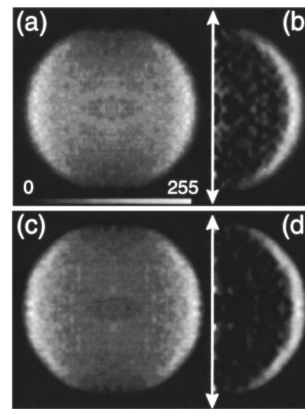


FIG. 3. (a) Data image of the Cl(²P_{3/2}) photofragment generated from the photodissociation of Cl₂ at 3.400 eV and detected using (2+1) REMPI. (b) Reconstruction of the data image in (a). (c) Data image of the Cl(²P_{3/2}) photofragment generated from the photodissociation of Cl₂ at 3.477 eV and detected using (3+1) REMPI. (d) Reconstruction of the data image in (c). Only half the image is presented in (b,d) since we have assumed azimuthal symmetry. The polarization direction of the photolysis laser is indicated by the arrow.

³⁵Cl* and ³⁵Cl are shown in Figures 2(a,c) and 3(a,c) respectively. The polarization direction of the photolysis laser is maintained parallel to the detector’s surface, such that reconstruction of the cylindrically symmetric 3D distribution from its 2D projection can be achieved through an inverse Abel transform.^{20,14,21} Both data images are averaged with respect to the symmetry axis (laser polarization direction) and subsequently averaged with respect to the center-of-symmetry.

The reconstructed images shown in Figures 2(b,d) and 3(b,d) represent the intensity profile of planar cuts through the 3D distributions along the symmetry axis, i.e., they are equivalent to polar plots of the photofragment angular distributions $I(\rho, \theta)$, where ρ is the distance from the center of the image and θ the polar angle with respect to the symmetry axis. Prior to reconstruction, the data image is smoothed by sweeping a 2D Gaussian mask (9×9 pixels, half-width 5 pixels) across the entire image (noise filtering). The radial position ρ of the photofragments is related to its speed u via the relationship

$$\rho = ut, \quad (2)$$

where t is the flight time of the photofragment from the interaction region to the detector. Time t is essentially a constant for all speeds as the laboratory extraction energy (0.5–2.5 keV) is much greater than the center-of-mass energy of the photofragments (typically 0.5–3 eV). Because of the azimuthal symmetry, the 3D radial intensity distribution is determined from the reconstructed image using the relationship^{14,21}

$$I(\rho) = 2\pi \sum_{\theta=0}^{\pi} I(\rho, \theta) \rho \sin \theta, \quad (3)$$

which upon change of variables yields the translational energy distribution $I(E)$

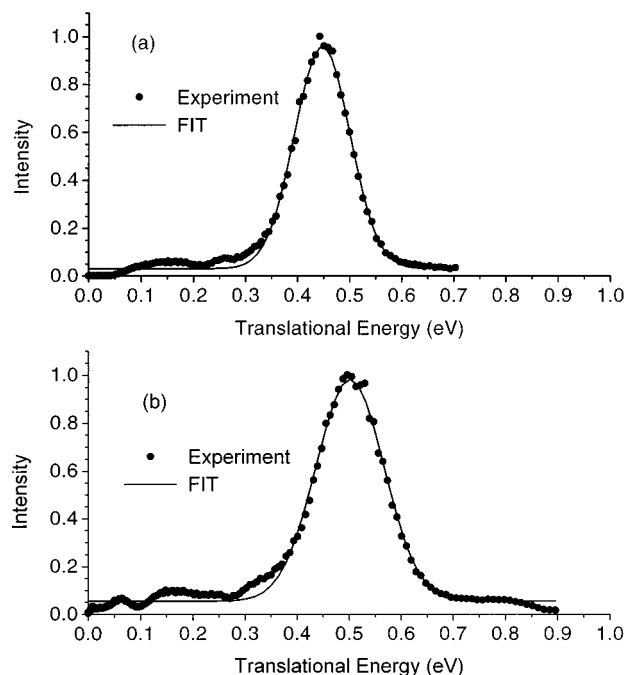


FIG. 4. (a) Translational energy distribution for the Cl(²P_{1/2}) photofragment generated from the photodissociation of Cl₂ at 3.40 eV. (b) Translational energy distribution for the Cl(²P_{3/2}) photofragment generated from the photodissociation of Cl₂ at 3.40 eV.

$$I(E) = I(\rho) \frac{d\rho}{dE}, \quad (4)$$

$$I(E) = \left(\frac{t^2}{m}\right) \frac{I(\rho)}{\rho} = \left(\frac{2\pi t^2}{m}\right) \sum_{\theta=0}^{\pi} I(\rho, \theta) \sin \theta. \quad (5)$$

The translational energy distributions for the Cl and Cl* photofragments determined using Eq. 5 on the reconstructed images of Figures 2, 3 are shown in Figure 4.

The angular distributions for Cl* and Cl photofragments shown in Figures 5(a, b), are determined by integrating the reconstructed images in Figures 2(b) and 3(b) from $\theta=0$ to π , along 5° radial-sector strips with radii and widths identical to the position and width of the corresponding peaks in the translational energy distributions. Both distributions are strongly anisotropic, that of Cl* peaking at $\theta=0^\circ$ and 180° while the maximum intensity of the Cl distribution occurs at $\theta=90^\circ$.

IV. DISCUSSION

A. Cl* production

Inspection of both data images in Figures 2(a,c) indicate that most of the photofragments are ejected along the polarization direction of the photolysis laser. Modeling the experimental angular distribution presented in Figure 5(a) using the functional form of Eq. 1 we find that $\beta(^2P_{1/2}) = 1.78 \pm 0.05$. This value is consistent with the expectations of a prompt dissociation following excitation through a parallel transition^{6,7} such as the $0_u^+ \leftarrow 0_g^+$ ($X^1\Sigma_g$). The slight variation from the $\beta=2$ value expected for a perfect parallel tran-

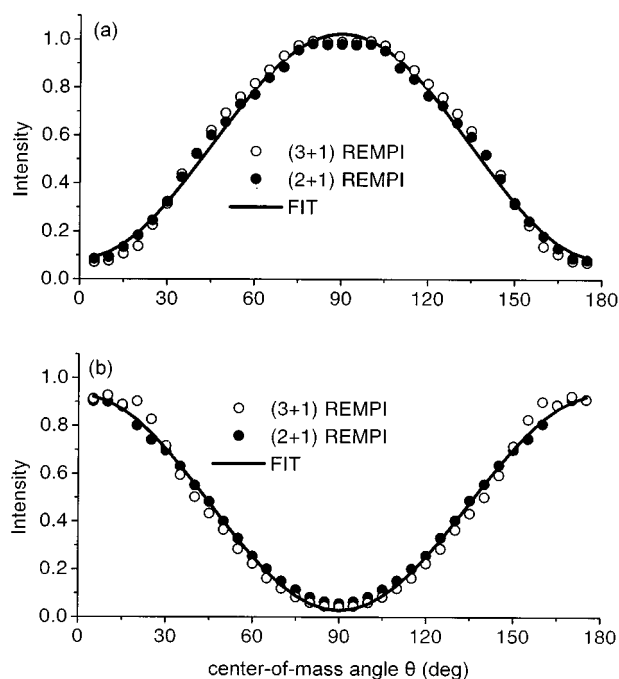


FIG. 5. (a) An angular distribution for the Cl(²P_{1/2}) photofragment generated from the photodissociation of Cl₂. (b) Angular distribution for the Cl(²P_{3/2}) photofragment generated from the photodissociation of Cl₂.

sition is discussed later in the text. Our observations agree with the assignments presented in the introduction, as well as with previous measurements of Kawasaki and co-workers⁴ who reported $\beta(^2P_{1/2}) = 1.80 \pm 0.20$. One of the advantages of the ion imaging technique over Doppler spectroscopy is that we can simultaneously measure the translational energy distributions of the photofragments and the angular distribution. For Cl* we can calculate the dissociation energy of Cl₂($X^1\Sigma_g$) using the relationship

$$E_T = \frac{m(\text{Cl})}{m(\text{Cl}_2)} [E_{ph} - \Delta E_{S.O.} - D_0], \quad (6)$$

where E_T is the translational energy of the photofragment, $\Delta E_{S.O.} = 0.109$ eV is the spin orbit splitting and D_0 the dissociation energy of Cl₂($X^1\Sigma_g$). Upon substitution we find that $D_0 = 2.474 \pm 0.020$ eV which is in excellent agreement with the spectroscopically determined value.²²

B. Cl production

The data images of Figures 3(a,d) obtained using the (2+1) and (3+1) REMPI detection appear as circular disks with most of the intensity along the equator, yet appreciable intensity throughout the surface of the disk. The angular distributions shown in Figure 5(b) are derived from the reconstructed images in Figures 3(b,d) using the procedure described earlier. Fitting this distribution to a functional form of Eq. 1 we find that $\beta(^2P_{3/2}) = -0.87 \pm 0.05$ irrespective of the detection method.

As we mentioned in the introduction, if Cl is produced exclusively by the $1_u \leftarrow 0_g^+$ ($X^1\Sigma_g$) excitation, then assuming

that the 1_u state is purely repulsive, the prompt dissociation will yield a $\sin^2\theta$ Cl atom distribution (i.e., $\beta(^2P_{3/2}) = -1.0$). Consequently our deviation from this prediction can be caused by one of the following two reasons: (a) The lifetime of the excited state is long enough to smear out the pure $\sin^2\theta$ shape of the distribution.^{6,7} (b) The absorption coefficient $\epsilon(0_u^+)$ for the $B(0_u^+) \leftarrow 0_g^+$ ($X^1\Sigma_g^+$) transition, is significant with respect to $\epsilon(1_u^+)$ the absorption coefficient for the $1_u \leftarrow 0_g^+$ ($X^1\Sigma_g^+$) process, such that enough Cl(1_u) photofragments are produced with a $\cos^2\theta$ distribution that cause an effective anisotropy parameter of -0.87 . As theoretical predictions favor a purely repulsive 1_u state,^{23,24} we believe that the correct explanation is (b). To determine the branching ratio $B = [Cl(0_u^+)][Cl(1_u)]$, we fit the angular distribution using a functional form

$$I(\theta) = A(\sin^2\theta + B\cos^2\theta) \quad (7)$$

and find that $B = 0.088 \pm 0.030$ and consequently²⁵ $[Cl^*]/[Cl] = 8 \pm 1\%$. As there is one Cl(0_u^+) atom produced by the $B(0_u^+) \leftarrow 0_g^+$ ($X^1\Sigma_g^+$) process versus two Cl(1_u) atoms produced by the $1_u \leftarrow 0_g^+$ ($X^1\Sigma_g^+$) transition, the ratio of the absorption coefficients is $\epsilon(0_u^+)/\epsilon(1_u) = 0.18 \pm 0.06$.

Previous measurements of the Cl angular distribution reported $\beta(^2P_{3/2}) = -1.0 \pm 0.1$ at 3.49 eV by Kawasaki and coworkers,⁴ $-0.8 \geq \beta(^2P_{3/2}) \geq -1$ at 3.53 eV by Arikawa and coworkers,¹¹ while fitting the angular distribution reported by Adler and co-workers⁹ at 3.57 eV we find $\beta(^2P_{3/2}) = -0.82 \pm 0.06$. Both Kawasaki's and Arikawa's experiments involved Doppler profile analyses of the Cl and Cl* photofragment velocities, while Adler used photofragment recoil spectroscopy. Our $\beta(^2P_{3/2})$ value is in close agreement with these experiments, however, our $[Cl^*]/[Cl]$ branching ratio is approximately 5 times larger than the 0.016 ± 0.001 value determined for the energy studied in this experiment.⁴

In Figure 6 we present the potential energy curves involved in the photofragmentation of Cl₂ in the near UV region. The potential energy curves for the $X(0_g^+)$, $B(0_u^+)$ states are Morse potential fits to experimental spectroscopic constants² while the $C(1_u)$ curve has been adapted from Gibson *et al.*²³ We note that upon a vertical transition from the ground vibrational level of $X(0_g^+)$, we expect that the maximum absorption intensity will occur between 3 and 4 eV. Qualitatively, the fact that at higher energies $\epsilon(1_u) > \epsilon(0_u^+)$ while at lower energies the two absorption coefficients become comparable is consistent with the shape of these curves. In addition, the fact that the 1_u , 0_u^+ curves are essentially parallel between the energy range of 3.5 and 6 eV suggests that within the Franck–Condon approximation we can expect the ratio $\epsilon(1_u)/\epsilon(0_u^+)$ to remain nearly constant in this energy range. Evidence of curve crossing has been reported⁴ and is suggested by the reduction of the $\beta(^2P_{1/2})$ value from the perfect parallel transition value 2, to our experimentally observed value of 1.78. We hope that this report will stimulate detailed quantum mechanical calculations of the excited electronic states of molecular chlorine, which we believe will be instrumental in resolving some of the ques-

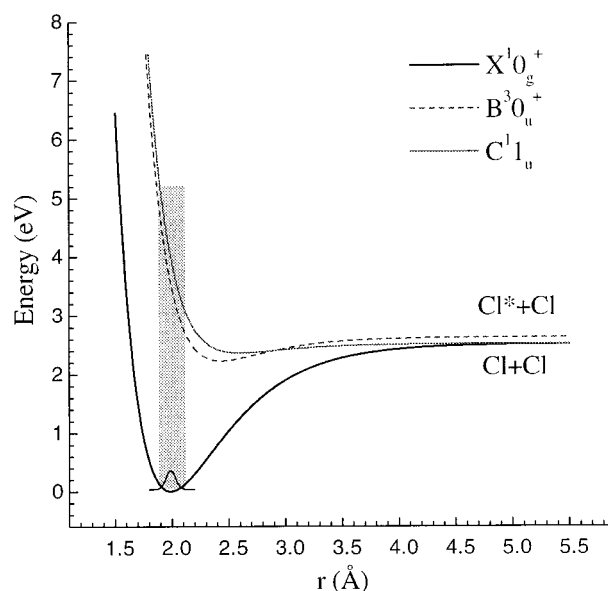


FIG. 6. Potential energy curves responsible for the absorption spectrum of Cl₂ in the near ultraviolet region. The shaded area indicates the region of greatest absorption intensity.

tions raised by the slight disagreement between the ion imaging and the Doppler experimental results.

ACKNOWLEDGMENTS

T.N.K. would like to acknowledge M. Lourakis of the Institute of Computer Science at FORTH for compiling the data acquisition software. This work is supported by the General Secretariat for Research and Technology under the program PENED94 and is conducted at the Ultraviolet Laser Facility operating at FORTH-IESL (Human Capital and Mobility, Access to Large Scale Facilities EU program, Contract No. CHGE-CT92-007).

¹R.S. Mulliken, *Phys. Rev.* **36**, 1440 (1930).

²G. Herzberg, *Molecular Spectra and Molecular Structure I, Spectra of Diatomic Molecules* (Van Nostrand, New York, 1950), pp. 319–322.

³L. Li, R.J. Lipert, J. Lobue, W.A. Chupka, and S.D. Colson, *Chem. Phys. Lett.* **151**, 335 (1988).

⁴Y. Matsumi, K. Tonokura, and M. Kawasaki, *J. Chem. Phys.* **97**, 1065 (1992).

⁵Reference 2, p. 224.

⁶R.N. Zare, *Mol. Photochem.* **4**, 1 (1972).

⁷S. Yang and R. Bersohn, *J. Chem. Phys.* **61**, 4400 (1974).

⁸G.E. Busch, R.T. Mahoney, R.I. Morse, and K.R. Wilson, *J. Chem. Phys.* **51**, 449 (1969).

⁹R.W. Diesen, J.C. Wahr, and S.E. Adler, *J. Chem. Phys.* **50**, 3635 (1969).

¹⁰S. Arepalli, N. Presser, D. Robie, and R.J. Gordon, *Chem. Phys. Lett.* **118**, 88 (1985).

¹¹Y. Matsumi, M. Kawasaki, T. Sato, T. Kinugawa, and T. Arikawa, *Chem. Phys. Lett.* **155**, 486 (1989).

¹²S. Deshmukh and W.P. Hess, *J. Photochem. Photobiol. A* **80**, 17 (1994).

¹³D.W. Chandler and P.L. Houston, *J. Chem. Phys.* **87**, 1445 (1987).

¹⁴A.J.R. Heck and D.W. Chandler, *Annu. Rev. Phys. Chem.* **46**, 335 (1995).

¹⁵P.L. Houston, *J. Phys. Chem.* **100**, 12757 (1996).

¹⁶D. Proch and T. Trickl, *Rev. Sci. Instrum.* **60**, 713 (1989).

¹⁷A threshold pixel value is set, which is determined by the CCD dark and readout noise as well as the residual ambient light. Pixel positions with intensity values below this threshold are ignored.

- ¹⁸C.E. Moore, *Atomic Energy Levels as Derived from the Analyses of Optical Spectra* (US GPO, Washington, DC, 1949).
- ¹⁹W.R. Simpson, T.P. Rakitzis, A.A. Kandel, J. Orr-Ewing, and R.N. Zare, *J. Chem. Phys.* **103**, 7313 (1995).
- ²⁰R.N. Barcewell, *Aust. J. Phys.* **9**, 198 (1956).
- ²¹D.W. Chandler, T.N. Kitsopoulos, M.A. Buntine, D.P. Baldwin, R.I. McKay, A.J.R. Heck, and R.N. Zare, *Gas-Phase Chemical Reaction Systems: Experiments and Models 100 Years after Max Bodenstein*, edited by J. Wolfrum, H.-R. Volpp, R. Rannacher, and J. Warnatz [Springer Series in Chem. Phys. (Springer Berlin, Heidelberg, 1996)].
- ²²K.P. Huber and G. Herzberg, *Constants of Diatomic Molecules* (Van Nostrand, New York, 1979), p. 146.
- ²³G.E. Gibson, O.K. Rice, and N.S. Bayliss, *Phys. Rev.* **44**, 193 (1933).
- ²⁴Reference 2, p. 392.
- ²⁵[Cl*]=[Cl(0_u⁺)] and [Cl]=[Cl(0_u⁺)]+[Cl(1_w)].